Dyes and Pigments 239 (2025) 112776

Contents lists available at ScienceDirect

Dyes and Pigments

journal homepage: www.elsevier.com/locate/dyepig

Synthesis and photophysical properties of π-extended carboxyl BODIPYs: An experimental and theoretical study

Gökhan Sevinç [a,*], Elif Akhüseyin Yıldız [b], Zeliha Pınar Taşkıran [a], Ahmet Karatay [b,**]

[a] Department of Chemistry, Faculty of Science, Bilecik Seyh Edebali University, TR, 11100, Bilecik, Turkey
[b] Department of Engineering Physics, Faculty of Engineering, Ankara University, 06100, Ankara, Turkey

ARTICLE INFO

Keywords:
Absorption
Carboxy-BODIPY
DFT
Fluorescence spectroscopy
Charge transfer

ABSTRACT

A series of new boron-dipyrromethenes (BODIPYs) bearing 4-carboxyphenyl unit at the *meso* (8) position of the BODIPY core have been successfully synthesized through the reactions of 2,4-diaryl substituted pyrroles with 4-formylbenzoic acid. The palladium-catalyzed Suzuki-Miyaura coupling reactions were performed on the *meso* unsubstituted BODIPY derivatives with 4-carboxyphenyl boronic acid to obtain distal and proximal substitution. Chemical structures were characterized using high resolution mass spectrometry (HRMS), $^{1}H/^{13}C$ NMR, and FTIR spectroscopy. The photophysical properties, excited state dynamics, and thermal degradation profiles were investigated in terms of aromatic subunits using electronic absorption/fluorescence measurements, femtosecond transient absorption spectroscopy, and thermogravimetric analysis (TGA), respectively. Experimentally investigated absorption and fluorescence properties, as well as structural features, were clarified using density functional theory (DFT) and electron-hole analysis. The absorption of the compounds ranges from 504 to 594 nm, and their emission ranges from 609 to 640 nm, depending on the aromatic groups at the BODIPY core. Performed pump probe spectroscopy measurements revealed that the excited state lifetime is shortened for 3,5 (proximal) positions compared to 1,7 (distal) positions due to increasing interactions between the molecular orbitals. The local n–π and π-π* excitations from DFT calculations and electron-hole analysis mainly characterize the electronic transitions, leading to limited intramolecular charge transfer to the BODIPY core. Charge transfer is highest at the 3,5-positions, decreases at the *meso* (8) position, and is lowest at the 1,7-positions of the BODIPY core. The newly developed BODIPYs with carboxyl groups show potential as agents in applications demanding extensive absorption and strong emission characteristics.

1. Introduction

Recently, there has been great interest in 4,4-difluoro-4-bora-3a,4a-diaza-*s*-indacene dyes (BODIPYs) (Fig. 1) as fluorescent molecules in diverse applications such as bioimaging [1–3], photodynamic therapy (PDT) [4–7], chemical sensors [8–11], dye-sensitized solar cells (DSSCs) [12–14] and light emitting diodes [15–17]. Thanks to their versatility in chemical modification, there are almost endless options for creating new compounds with desired properties. BODIPY compounds have high light absorption ($\varepsilon > 7 \times 10^4$ $M^{-1}cm^{-1}$) and fluorescence properties (Φ ca: 0.5–0.8) in the visible region spectrum. They also have a relatively small Stokes shift (around 10 nm). BODIPYs with various active chemical groups alter their general photophysical properties, crucial for their application success [18–22]

Carboxylic acid (-COOH) groups meet some requirements due to their binding abilities to the compounds. For example, carboxylic acid subunits are essential for covalent bonding to semiconducting surfaces in photovoltaic systems such as dye-sensitized solar cells [13,23–25]. Similarly, carboxyl groups are important in bioimaging applications and quantitative analyses where fluorophore-amino acid interactions are required. In this respect, the presence of carboxyl groups in the BODIPY core may be considered as a feasible way to make BODIPY chromophores more useful while preserving their photophysical properties.

Despite the novel synthetic versatility of BODIPYs and the abundance of approaches in the literature, there are still synthetic limitations in introducing both carboxylic acid and substituted aryl functionalities at the 1,7 (distal) and 3,5 (proximal) positions of the BODIPY core. Thus, although the BODIPY fluorophores have been widely studied,

* Corresponding author.
** Corresponding author.
E-mail addresses: gokhan.sevinc@bilecik.edu.tr (G. Sevinç), akaratay@eng.ankara.edu.tr (A. Karatay).

https://doi.org/10.1016/j.dyepig.2025.112776
Received 18 January 2025; Received in revised form 19 March 2025; Accepted 20 March 2025
Available online 22 March 2025

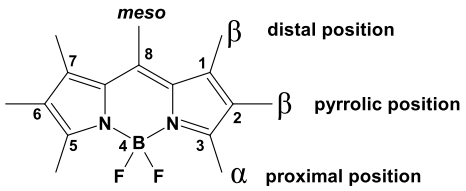

Fig. 1. Borondipyrromethene (BODIPY) core structure, IUPAC numeration and, positions on it.

photophysical, thermal properties and excited state dynamics of the carboxyphenyl appended BODIPYs have rarely been systematically studied in terms of substitution position on the BODIPY skeleton (Fig. 1) [26,27]. The literature indicates that aryl groups positioned at the *meso* (8) location exert only a minimal impact on the optical properties of BODIPYs. Attributed to the orthogonal orientation of the *meso*-phenyl moiety in relation to the planar BODIPY core, this configuration reduces the conjugation between the two units [22,28].

In this study, to enhance the conjugation as well as the extent of absorption and fluorescence, 2,4-aryl substituted pyrrole derivatives were employed to synthesize *meso*-carboxyphenyl BODIPYs in the initial series (compounds **B2**–**B4**). **B1** was synthesized from the pyrrole as a reference compound. To further enhance absorption and fluorescence, we synthesized meso-unsubstituted BODIPYs (**U1** and **U2**) by connecting two aryl-pyrrole derivatives; these compounds contain 4-bromophenyl groups at the distal (1,7) or proximal (3,5) positions of the BODIPY core (Fig. 1) that allow the addition of carboxyphenyl groups via Pd catalyzed Suzuki-Miyaura coupling reactions. In order to ascertain the effect of distal (1,7) and proximal (3,5) positions of the BODIPY core on the photophysical characteristics, 4-bromophenyl groups were methodically appended at the proximal positions in **U1** and at the distal positions in **U**2. Thus, we synthesized the resulting BODIPYs **B5** and **B6** with carboxybiphenyl groups, eliminating the conjugation-limiting *meso* group.

In summary, to expand the arsenal of the BODIPY tool, novel BODIPY derivatives including 4-carboxyphenyl and 4-carboxybiphenyl subunit (s) at the *meso* (8) or distal/proximal positions of the BODIPY core were designed and synthesized. We examined the influence of related groups on photophysical properties of the BODIPYs by systematically changing the positions of the carboxy-aryl groups on the BODIPY core (Fig. 1). We detailed the experimental spectroscopic properties of the compounds with density functional theory (DFT/TD-DFT) data including intramolecular charge transfers by electron-hole analysis. Also, since the thermal properties of the compounds can be an important parameter, especially in areas requiring high temperatures, we determined the thermal profiles of the resulting chromophores.

2. Experimental section

2.1. General information

All reactive and spectroscopic grade solvents were purchased from Merck and used without applying further purification techniques. Reactions were controlled with thin layer chromatography using Merck TLC Silica gel 60 F_{254}. Column chromatography was performed using silica gel 60 (particle size: 230–400 mesh). The melting points were measured on a SMP30 Stuart apparatus. HRMS spectra were recorded on Agilent 6224 LC/MS High Resolution Mass Time-of-Flight (HRMS) spectrometer in positive or negative mode. ^{1}H NMR spectra were taken on a Bruker Avance spectrometer in DMSO-d_6 with TMS as an internal standard at room temperature. The coupling constants (*J*) were reported in Hertz. ^{13}C NMR spectra were recorded directly using VARIAN Mercury spectrometer. Thermogravimetric analysis (TGA) of the BODIPYs were carried out by heating the compounds with Exstar SII TGA/DTA 7200 device under nitrogen flow with a heating rate of 10 °C/min in the range of 20–1100 °C. 2,4-diaryl-1*H*-pyrrole derivatives were prepared according to the literature procedure [29–32].

2.2. Optical measurements

A Perkin–Elmer 100 spectrometer (equipped with an ATR unit) was used for FT-IR spectra of compounds in the range of 650–4000 cm^{-1}. The Shimadzu UV-1800 model scanning spectrophotometer was used to obtain UV–VIS absorption spectra of the compounds in THF solvent. The emission characteristics of the compounds were analyzed using a PerkinElmer LS 55 fluorescence spectrophotometer. All solutions were kept in the dark and at room temperature. The UV/Vis and fluorescence measurements were taken within 8 h after the solution preparation. The BODIPY dyes were excited at maximum absorption wavelengths obtained from their UV–Vis spectra. Fluorescence quantum (Φ_F) yields were computed according to the formula given below (Eq. (1)) using Fluorescein ($\Phi_F = 0.79$ in ethanol) [33].

$$\Phi_F = \Phi_F(\mathrm{Std})\,\frac{F\,.\,A_{Std}\,.\,n^2}{F_{Std}\,.\,A\,.\,n^2_{Std}} \qquad \text{(Eq. 1)}$$

In the equation; Φ_F: quantum efficiency of the sample, Φ_F(Std): quantum yield of the reference, F: area under the fluorescence emission curves of the sample, F_{Std}: area under the fluorescence emission curves of the standard, A_{Std}: absorbance value of the standard at excitation wavelength, A: absorbance value of the sample at excitation wavelength, n: refractive index of the solvent used in solving and n_{Std}: refractive index of the solvent used in solving the standard.

A Ti: sapphire laser amplifier, an optical parametric amplifier system with a pulse duration of 45 fs and a repetition rate of 1 kHz, was used to perform femtosecond transient absorption spectroscopy measurements (Spectra-Physics, Spitfire Pro XP, TOPAS). A commercial pump-probe experimental setup (Spectra-Physics, Helios) with a white-light continuum probe was used to study the impact of electron donor qualities and the excited state lifetime. The pump wavelength for ultrafast pump-probe spectroscopy investigations was determined based on the maximum absorption wavelength of the investigated compounds. Surface Xplorer software from Ultrafast System was used to analyze all data.

2.3. Computational methods

The DFT calculations were performed using the Gaussian 09 program [34]. The ground state geometry optimizations of the designed BODIPY derivatives and the excited-state calculations were performed in the frameworks of DFT and time-dependent DFT (TDDFT). The B3LYP exchange-correlation function was chosen together with the 6-311G basis set for structural optimization using the Conductor-like Polarizable Continuum model (CPCM) in THF. The vibrational frequencies were computed to check whether the optimized structures were in global minima and no negative frequencies were found. Time-dependent DFT (TDDFT) was employed to calculate excited-state properties of the dyes by using B3LYP exchange-correlation functional and the Los Alamos effective core potential basis set (LANL2DZ) in THF. Empirical force dispersion term (Grimme DFT-D3) were used via the *IOp(3/124 = 30)* functional. Natural transition orbitals (NTOs) [35] were calculated obtained from the transition density matrices calculated by TDDFT using Multiwfn [36]. Hole-electron analysis of the compounds was performed with the same software based on the first excited-state energies from the TDDFT calculations. The density of states (DOS) diagrams were generated utilizing the Gauss–Sum v3.0 program [37].

2.4. Synthesis of the BODIPYs

2.4.1. 4,4-Difluoro-8-[4-carboxyphenyl]-4-bora-3a,4a-diaza-s-indacene (B1)

A solution of N_2 degassed DCM (100 mL), pyrrole (150 μL, 2.2

mmol), and 4-carboxybenzaldehyde (150 mg, 1.00 mmol) was prepared, to which trifluoroacetic acid (50 μL) was subsequently added as a catalyst. The mixture was covered with aluminum foil and stirred overnight at room temperature. TLC showed depletion of the aldehyde (4:1 $CHCl_3$/EtOH, v/v). The oxidizing agent 2,3-Dichloro-5,6-dicyano-*p*-benzoquinone (340 mg 1.50 mmol) was added to the mixture and stirred for 30 min. At the end of this period, the reaction mixture was placed in an ice bath and the temperature was reduced to 0 °C. Then, *N,N*-diisopropylethylamine (1.16 mL, 7.0 mmol) was added to the mixture by portions of 100 μL volumes with vigorous stirring. The mixing was continued for another half hour in the cold after the addition. Subsequently, $BF_3{\cdot}OEt_2$ (1.40 mL, 11.0 mmol) was added by portions of 100 μL volumes with vigorous stirring. After the reaction mixture was stirred in an ice bath for 2 h, the ice bath was removed and stirred at room temperature overnight. Pure water (50 mL) was slowly added to the reaction mixture and mixed for 10 min. The organic phase was separated from the mixture taken into the separating funnel, the solvent was removed in a rotary evaporator, and the compound **B1** was purified through a silica gel column using chloroform and then chloroform/ethanol (4:1, v/v). Yield: 128 mg (41 %), mp: 188–189 °C. FTIR (ATR, cm^{-1}) ν_{max}: 1686, 1571, 1543, 1418, 1390, 1289, 1261, 1114, 1074, 973, 915, 752, 727. ^{1}H NMR (400 MHz, DMSO-d_6) δ[ppm]: 8.17 (s, 2H), 8.13 (d, $J = 8.0$ Hz, 2H), 7.78 (d, $J = 8.4$ Hz, 2H), 7.03 (d, $J = 8.4$ Hz, 2H), 6.70 (d, $J = 6.0$ Hz, 2H). ^{13}C NMR (100 MHz DMSO-d_6) δ: 166.5, 145.5, 145.2, 136.8, 134.0, 132.8, 131,7, 130,6, 129.3, 119.4. HRMS (Q-TOF-ESI) (*m/z*) Calcd: 312.08818 ($C_{16}H_{11}BF_2N_2O_2$), found: 311.0842 $[M-H]^-$.

2.4.2. 4,4-difluoro-8-[4-carboxyphenyl]-1,3,5,7-tetraphenyl-4-bora-3a,4a-diaza-s-indacene (B2)

To a solution of 4-carboxybenzaldehyde (100 mg, 0.67 mmol) and 2,4-diphenyl-1*H*-pyrrole (320 mg, 1.47 mmol) in DCM (60 mL) a few drops of trifluoroacetic acid (TFA) and *p*-Chloranil (0,25 g, 1,02 mmol) were added, and the reaction was stirred overnight. Complete consumption of the aldehyde was verified by TLC. The reaction mixture was concentrated to about 25 mL on evaporator and filtered through a filter paper. The green filtrate was washed with water, extracted with $CHCl_3$ (3 × 30 mL) and the solvent evaporated. The solid, which was thoroughly dried in a vacuum oven, was dissolved in DCM (100 mL), placed in an ice bath and the temperature was reduced to 0 °C. Then, *N,N*-diisopropylethylamine (770 μL, 4.67 mmol) was added dropwise to the mixture and stirred 30 min. Subsequently, $BF_3{\cdot}OEt_2$ (930 μL, 7.33 mmol) was added by portions of approximately 100 μL volumes with vigorous stirring. After the reaction mixture was stirred in an ice bath for 2 h, the ice bath was removed and stirred at room temperature overnight. Pure water (100 mL) was slowly added to the reaction mixture and mixed for 10 min. The organic phase was separated from the mixture taken into the separating funnel, the solvent was removed in a rotary evaporator, and the compound **B2** was purified through a silica gel column using chloroform and then chloroform/ethanol (9:1, v/v). Yield: 160 mg (39 %), mp: 298–299 °C. FTIR (ATR, cm^{-1}) ν_{max}: 2922, 2848, 1681, 1541, 1492, 1473, 1296, 1226, 1168, 1137, 1027, 838, 759, 691. ^{1}H NMR (400 MHz, DMSO-d_6) δ[ppm]: 7.88-7.86 (m, 4H), 7.49-7.48 (m, 6H), 7.07-7.01 (m, 4H), 6.91 (d, $J = 7.2$ Hz, 2H), 6.86-6.76 (m, 8H), 6.76 (s, 2H). ^{13}C NMR (125 MHz DMSO-d_6) δ: 166.9, 157.0, 151.9, 148.3, 145.8, 139.7, 135.1, 132.5, 131.1, 130.2, 129.8, 129.1, 128.7, 127.5, 126.9, 125.4, 124.1, 121.2. HRMS (Q-TOF-ESI) (*m/z*) Calcd: 616.21338 ($C_{40}H_{27}BF_2N_2O_2$), found: 615.2092 $[M-H]^-$.

2.4.3. 4,4-difluoro-8-[4-carboxyphenyl]-1,3,5,7-[4-methoxyphenyl]-4-bora-3a,4a-diaza-s-indacene (B3)

The reaction was carried out applying the same procedure used for the synthesis of the compound **B2**, starting with 4-carboxybenzaldehyde (100 mg, 0.67 mmol) and 2,4-bis[4-methoxyphenyl]-1*H*-pyrrole (410 mg, 1.47 mmol). Purification on silica gel using chloroform and then chloroform/ethanol (9:1, v/v) afforded 100 mg of **B3** (yield 20 %), mp: 302–303 °C. FTIR (ATR, cm^{-1}) ν_{max}: 2962, 2921, 1689, 1608, 1470, 1435, 1255, 1234, 1145, 1028, 825, 747. ^{1}H NMR (400 MHz, DMSO-d_6) δ[ppm]: 7.87 (d, $J = 8.8$ Hz, 4H), 7.09 (d, $J = 7.6$ Hz, 2H), 7.04 (d, $J = 8.4$ Hz, 4H), 6.97 (d, $J = 8.4$ Hz, 2H), 6.87 (s, 2H), 6.70-6.68 (m, 4H), 6.38 (d, $J = 8.4$ Hz, 4H), 3.84 (s, 6H), 3.55 (s, 6H). ^{13}C NMR (125 MHz DMSO-d_6) δ: 167.1, 161.0, 158.4, 156.2, 151.9, 147.5, 146.1, 143.6, 143.2, 139.7, 132.5, 131.6, 130.3, 128.8, 128.5, 125.4, 114.2, 113.2, 55.8, 55.4. HRMS (Q-TOF-ESI) (*m/z*) Calcd: 736.2556 ($C_{44}H_{35}BF_2N_2O_6$), found: 735.2531 $[M-H]^-$.

2.4.4. 4,4-difluoro-8-[4-carboxyphenyl]-1,7-[1-naphtyl]-3,5-[4-methoxyphenyl]-4-bora-3a,4a-diaza-s-indacene (B4)

The reaction was performed applying the same procedure used for the synthesis of the **B2**, starting with 4-carboxybenzaldehyde (100 mg, 0.67 mmol) and 2-(4-methoxyphenyl)-4-(1-naphtyl)-1*H*-pyrrole (480 mg, 1.47 mmol). Purification on silica gel using chloroform and then chloroform/ethanol (9:1, v/v) afforded 230 mg of **B4** (yield 44 %), mp: 291–292 °C. FTIR (ATR, cm^{-1}) ν_{max}: 2954, 1689, 1604, 1478, 1432, 1260, 1134, 1033, 797, 748, 625, 551. ^{1}H NMR (400 MHz, DMSO-d_6) δ[ppm]: 7.95 (d, $J = 8.4$ Hz, 4H), 7.70-7.64 (m, 1H), 7.50-7.41 (m, 4H), 7.34-7.25 (m, 6H), 7.06 (d, $J = 9.2$ Hz, 4H), 6.99-6.97 (m, 2H), 6.94 (d, $J = 7.6$ Hz, 1H), 6.92-6.90 (m, 1H), 6.82-6.65 (m, 3H), 6.27 (d, $J = 8.4$ Hz, 1H), 5.97 (d, $J = 8.4$ Hz, 1H), 3.84 (s, 6H). ^{13}C NMR (125 MHz DMSO-d_6) δ: 166.3, 161.1, 156.6, 144.8, 133.5, 132.8, 132.7, 132.6, 131.7, 131.5, 131.3, 130.6, 129.8, 128.7, 127.9, 127.7, 126.4, 126.2, 124.7, 124.5, 114.3, 55.8. HRMS (Q-TOF-ESI) (*m/z*) Calcd: 776.2658 ($C_{50}H_{35}BF_2N_2O_4$), found: 775.2641 $[M-H]^-$.

2.4.5. 4,4-Difluoro-1,7-phenyl-3,5-[4-bromophenyl]-4-bora-3a,4a-diaza-s-indacene (U1)

A mixture of DMF (0.4 mL, 5.14 mmol) and $POCl_3$ (0.35 mL, 5.14 mmol) was stirred in an ice bath for 5 min. After being warmed to room temperature, it was stirred for an additional 20 min. After this period, the temperature was again reduced to −4 °C using an ice/salt bath, and dichloroethane (2 mL) was added dropwise to the reaction. Then, 2-(4-bromophenyl)-4-phenyl-1*H*-pyrrole (0.9 g, 3.02 mmol) dissolved in dichloroethane (5 mL) was added dropwise. When the addition was completed, the ice bath was removed and the solution was refluxed at 90 °C for 30 min. Then, the solution was cooled to room temperature, saturated NaOAc (10 mL) solution was added and refluxed again for 30 min. At the end of this period, the reaction mixture was transferred to the separation funnel and the organic phase was separated. The aqueous phase was extracted with dichloromethane (20 mLx2), combined with the organic phase, and the solvents were evaporated. The solid, dried at room temperature in a vacuum oven, was dissolved in 15 mL dichloromethane (DCM) and cooled to −4 °C using an ice/salt bath. Then, $POCl_3$ (350 μL) was added by portions of 50 μL volumes with vigorous stirring. The ice bath was removed and the mixture was stirred at room temperature overnight. Then, *N,N*-diisopropylethylamine (1.00 mL, 6.06 mmol) and $BF_3{\cdot}OEt_2$ (1.00 mL, 7.88 mmol) were added and stirred for 24 h at room temperature. Subsequently, pure water (50 mL) was slowly added to the reaction mixture and stirred for 10 min. The organic phase was extracted with chloroform (30 mLx3). The solvent was removed in a rotary evaporator and purification on silica gel using chloroform and then chloroform/ethanol (9:1, v/v) afforded 205 mg of **U1** (yield 21 %), mp: 278–279 °C. FTIR (ATR, cm^{-1}) ν_{max}: 3433, 3067, 2921, 1684, 1592, 1549, 1480, 1446, 1237, 1073, 1008, 830, 764, 696. ^{1}H NMR (500 MHz, $CDCl_3$) δ[ppm]: 7.79 (d, $J = 8.0$ Hz, 4H), 7.57 (d, $J = 8.0$ Hz, 4H), 7.45–7.43 (m, 6H), 7.02-6.99 (m, 5H), 6.63 (s, 2H). HRMS (Q-TOF-ESI) (*m/z*) Calcd: 654.01122 ($C_{33}H_{21}BBr_2F_2N_2$), found: 655.0161 $[M+H]^-$.

2.4.6. 4,4-Difluoro-1,7-[4-bromophenyl]-3,5-phenyl-4-bora-3a,4a-diaza-s-indacene (U2)

The reaction was carried out applying the same procedure used for the synthesis of the compound **U1**, starting with 4-(4-bromophenyl)-2-phenyl-1*H*-pyrrole (0.9 g, 3.02 mmol). Purification on silica gel using

chloroform and then chloroform/ethanol (9:1, v/v) afforded 140 mg of **U2** (yield 14 %), mp: 295–296 °C. FTIR (ATR, cm^{-1}) ν_{max}: 3733, 3067, 2961, 1612, 1589, 1477, 1397, 1220, 1097, 1062, 1002, 805, 767, 684. ^{1}H NMR (500 MHz, $CDCl_3$) δ[ppm]: 7.95-7.93 (m, 4H), 7.65-7.64 (m, 4H), 7.52-7.51 (m, 2H), 7.47-7.46 (m, 4H), 7.39 (d, $J = 8.0$ Hz, 4H), 7.36 (s, 1H), 6.74 (s, 2H). HRMS (Q-TOF-ESI) (*m/z*) Calcd: 654.01122 ($C_{33}H_{21}BBr_2F_2N_2$), found: 655.0126 $[M+H]^-$.

2.4.7. 4,4-Difluoro-1,7-phenyl-3,5-[4-carboxybiphenyl]-4-bora-3a,4a-diaza-s-indacene (B5)

In a Schlenk flask, compound **U1** (40 mg, 0.061 mmol), 4-carboxyphenyl boronic acid (61 mg, 0.367 mmol), $[PdCl_2(PPh_3)_4]$ (4.3 mg, 6.1×10^{-3} mmol) and K_2CO_3 (51 mg, 0.367 mmol) were added to deaerated THF–H_2O (5 mL, 4:1, v/v) under N_2. The reaction mixture was heated at 90 °C for 12 h. After that the reaction was quenched by adding water (30 mL) and the mixture was extracted with $CHCl_3$ (30 mLx3). The solvent was removed in a rotary evaporator and the crude product was dried in a vacuum oven at room temperature. Purification on silica gel using chloroform and then chloroform/ethanol (9:1, v/v) afforded 21 mg of **B5** (yield 45 %), mp: 257–258 °C. FTIR (ATR, cm^{-1}) ν_{max}: 3379, 3153, 2925, 1683, 1611, 1585, 1512, 1419, 1356, 1325, 1268, 1193, 1127, 1045, 1016, 834, 762, 702. ^{1}H NMR (400 MHz, DMSO-d_6) δ[ppm]: 12.90 (s, 2H), 8.49-8.47 (m, 3H), 8.28 (s, 2H), 8.08 (t, $J = 8.4$ Hz, 6H), 8.04-8.01 (m, 5H), 7.93-7.89 (m, 3H), 7.73 (d, $J = 8.4$ Hz, 2H), 7.58 (t, $J = 8.4$ Hz, 2H), 7.54 (t, $J = 7.6$ Hz, 3H), 7.47 (t, $J = 7.2$ Hz, 2H), 7.18 (s, 1H). ^{13}C NMR (125 MHz DMSO-d_6) δ: 167.7, 156.4, 144.1, 139.0, 133.3, 132.5, 132.0, 131.9, 130.7, 130.5, 129.7, 129.3, 129.2, 129.0, 128.1, 127.4, 127.3, 115.3. HRMS (Q-TOF-ESI) (*m/z*) Calcd: 736.23452 ($C_{47}H_{31}BF_2N_2O_4$), found: 735.22701 $[M-H]^-$.

2.4.8. 4,4-Difluoro-3,5-phenyl-1,7-[4-carboxybiphenyl]-4-bora-3a,4a-diaza-s-indacene (B6)

The reaction was carried out applying the same procedure used for the synthesis of the compound **B5**, starting with the compound **U2** (90 mg, 0.138 mmol). Purification on silica gel using chloroform and then chloroform/ethanol (9:1, v/v) afforded 48 mg of **B6** (yield 47 %), mp: 288–289 °C. FTIR (ATR, cm^{-1}) ν_{max}: 3062, 1690, 1608, 1590, 1535, 1477, 1427, 1395, 1290, 1206, 1124, 1050, 1000, 869, 826, 768, 697. ^{1}H NMR (500 MHz, $CDCl_3$) δ[ppm]: 8.02-8.00 (m, 5H), 7.94-7.90 (m, 5H), 7.87 (d, $J = 5.2$ Hz, 6H), 7.83 (d, $J = 8.0$ Hz, 6H), 7.69 (s, 1H), 7.50-7.48 (m, 4H), 7.13 (s, 2H). ^{13}C NMR (125 MHz DMSO-d_6) δ: 167.7, 157.5, 145.1, 143.7, 140.0, 134.2, 132.9, 132.4, 132.0, 130.7, 130.5, 130.4, 130.0, 129.7, 128.8, 128.3, 127.3, 120.0. HRMS (Q-TOF-ESI) (*m/z*) Calcd: 736.23452 ($C_{47}H_{31}BF_2N_2O_4$), found: 735.23594 $[M-H]^-$.

3. Results and discussion

3.1. Synthesis and characterization

The BODIPY dyes **B1**–**B4** and **B5**–**B6** were prepared using the synthetic route depicted in Schemes 1 and 2, respectively.

The compounds were synthesized utilizing two distinct synthetic methodologies. The initial group comprises the compounds **B1** through **B4**, while the subsequent group includes **U1**, **U2**, **B5**, and **B6**. Bromine-substituted BODIPY derivatives, **U1** and **U2**, served as starting materials for the synthesis of **B5** and **B6**, respectively. The synthesis of compounds **B1–B4** was performed employing an acid-catalyzed one-pot approach involving aromatic aldehyde and pyrrole derivatives, a method extensively referenced in the literature [18,30]. The synthesis method under discussion is extensively documented in BODIPY literature [22]. However, in our initial experiments synthesizing **B2–B4**, the dipyrromethane intermediates failed to form using the established method, as indicated by thin layer chromatography. The issue was resolved by adding *p*-chloranil at the start of the reaction, based on a modification by Duan et al. [38], eliminating the need to wait for dipyrromethane intermediate formation. Soon after the acid catalyst was introduced, the dipyrromethene derivative was started to formation as a deep green color. The yields obtained for this series were 41 %, 39 %, 20 %, and 44 % for the compounds **B1** through **B4**, respectively. The presence of 4-methoxy groups at distal positions resulted in approximately a 50 % reduction in synthesis yield. In comparison to BODIPYs synthesized from aromatic aldehydes and alkyl-substituted pyrroles as precursors, the incorporation of 4-carboxyphenyl groups tends to enhance the yields. In contrast to the compounds under discussion, dyes **B5** and **B6** are distinguished by the absence of substituted groups at the *meso* (8) positions of the BODIPY core. Instead, they possess carboxylic acid groups located at the 3,5- and 1,7-positions for **B5** and **B6**, respectively. In the synthesis process, the initial step involved the formylation of pyrrole derivatives via the Vilsmeier-Haack reaction. This was succeeded by an exemplary method employing phosphorus oxychloride as a Lewis acid, as elucidated by Wu and Burgess [39], to produce the symmetrical *meso*-unsubstituted BODIPYs **U1** and **U2**. The synthesis yields of unsubstituted BODIPYs from formylated pyrrole derivatives were found to be 21 % and 14 % for **U1** and **U2**, respectively. These values are consistent with those reported in the literature [39]. In the concluding step, the Suzuki-Miyaura coupling reactions were executed employing 4-carboxyphenylboronic acid with a palladium catalyst. Consequently, the symmetrical and conjugation-enhanced borondipyrromethene compounds **B5** and **B6** were synthesized. The ultimate synthesis of compounds **B5** and **B6** resulted in yields of 45 % and 47 %, respectively. These yields are considered moderate and are characteristic of the outcomes typically observed in Suzuki–Miyaura coupling reactions involving BODIPY compounds [32,40].

The chemical structures were verified utilizing NMR, FTIR, and HRMS techniques, and the obtained data exhibited consistency with the proposed structures in each instance. The BODIPY compounds **B1–B4** have a carboxylic acid group (-CO_2H) at the *meso* (8) positions of the BODIPY core. In the ^{1}H NMR spectrum of **B1**, the peaks belonging to aromatic phenyl and pyrrole protons were observed as double peaks at 8.13, 7.78, 7.03, and 6.70 ppm. A broad peak belonging to the carboxyl (-CO_2H) proton was observed in the spectrum at 13.5 ppm. While the carboxyl peak was identified at 12.3 ppm in compound **B3** and 12.2 ppm

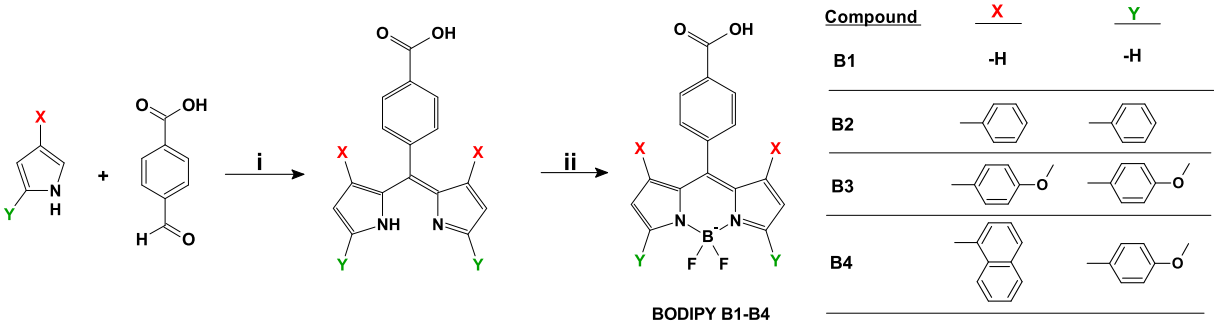

Scheme 1. The synthesis of the compounds **B1–B4. i**: Trifluoroacetic acid (cat.), *p*-Chloranil, DCM, rt, 24 h; **ii**: DIPEA (Hunig's base), $BF_3{\cdot}OEt_2$, DCM, 24 h, rt.

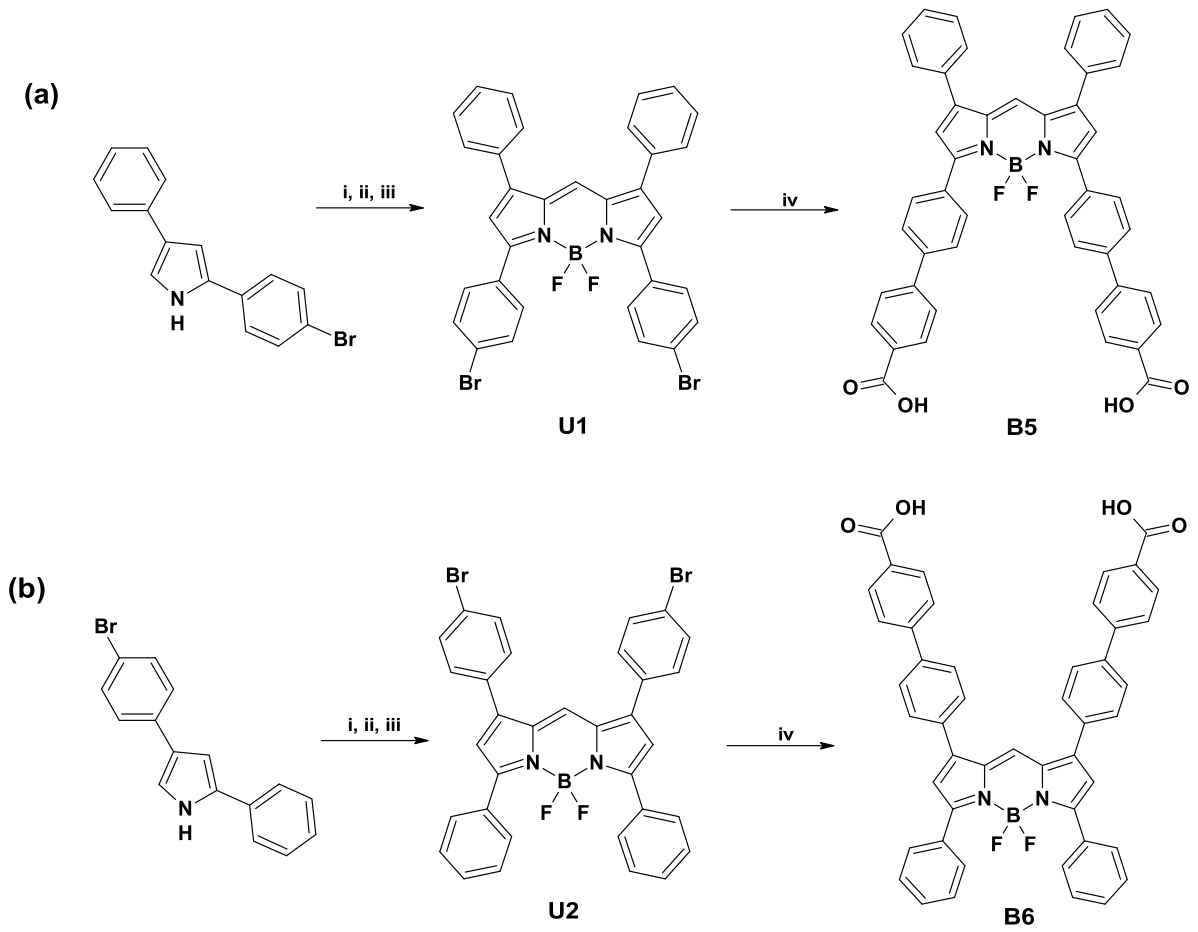

Scheme 2. The synthesis of the compounds **B5** (a) and **B6** (b). **i**: $POCl_3$/DMF, DCE, 0 °C; **ii**: $POCl_3$, DCM, 24 h, rt; **iii**: DIPEA (Hunig's base), $BF_3{\cdot}OEt_2$, DCM, 24 h, rt; **iv**: 4-carboxylphenylboronic acid, $[PdCl_2(PPh_3)_4]$, K_2CO_3, THF-H_2O, 90 °C, 12 h.

in compound **B4**, it was notably absent in **B2.** The pyrrole protons positioned at the 2,6 locations on the BODIPY core were detected as a singlet peak at 6.76 ppm for the compound **B2** and 6.87 ppm for the compound **B3**, each demonstrating 2H integration. This is compatible with the structure being symmetrical. The relevant peaks are included in multiple peaks in the other compounds in the series. The compounds contain intense phenyl and naphthyl groups. Consequently, the peaks manifested as multiplets within the 6–9 ppm range. The observed number of hydrogen atoms corresponds with the expected molecular structures. In the ^{13}C NMR spectra of the compounds, the carbonyl (C═O) carbon peaks were observed in the range of 167.7-166.5 ppm, the C═N carbon peaks in the range of 161.1-145.5 ppm, the characteristic C_β carbon peaks in the range of 158.4-144.1 ppm, and the methoxy (–OCH_3) carbon peaks in the range of 55.8-55.4 ppm. Additionally, the aromatic phenyl carbon peaks were observed within a broad range of approximately 156-113 ppm. With increasing electronegativity of substituent groups attached to the carbon atoms, a downfield shift in the peaks is observed. The detection of a singular peak for –OCH_3 carbons indicates the symmetrical nature of the BODIPYs.

The specific infrared absorptions (peaks) in the FTIR spectra of BODIPYs are given in Table 1. In the FTIR spectra of the compounds, the aromatic C–H stretching vibrations were observed at frequencies exceeding 3000 cm^{-1}, whereas the aliphatic C–H stretching vibrations were noted at frequencies below 3000 cm^{-1}. The C═N stretching vibrations were detected as minor sharp peaks within the frequency range of 1608–1697 cm^{-1}. These peaks were often observed combined with C═C peaks (1590-1635 cm^{-1}). B–F stretching vibrations were identified within the spectral range of 1073–1168 cm^{-1} in BODIPY derivatives. C–Br vibrations were observed as a clearly intense sharp peak in 762 and 764 cm^{-1} for the compounds **U1** and **U2**, respectively. The carbonyl (C═O) groups exhibited the most pronounced peaks in the FTIR spectra, appearing as highly intense peaks within a restricted range of 1681–1690 cm^{-1}. In the compounds **B5** and **B6**, the C–Br vibration peaks observed in **U1** and **U2** were replaced by carbonyl vibrations, indicating that coupling reactions occurred and resulted in the detachment of both bromine atoms from the compounds.

Table 1
FTIR wavenumbers (cm^{-1}) of the BODIPYs.

Compound	$\nu_{C=C}$	$\nu_{B\text{-}F}$	$\nu_{C\text{-}Br}$	$\nu_{C=N}$	$\nu_{C=O}$
B1	1571	1114	–	–	1686
B2	1541	1168	–	–	1681
B3	1608	1145	–	–	1689
B4	1604	1134	–	–	1689
U1	1592	1073	762	1684	–
U2	1589	1097	764	1612	–
B5	1585	1193	–	1611	1683
B6	1590	1124	–	1608	1690

3.2. Photophysical properties

The absorption and fluorescence spectra of the examined BODIPY compounds (**B1–B6**) were acquired in tetrahydrofuran (THF) at ambient temperature. The corresponding spectra of these dyes are illustrated in Fig. 2a–b, while the photophysical parameters are presented in Table 2. The absorption spectrum of compound **B1**, derived from pyrrole, exhibited the typical BODIPY profile [22,41], characterized by a

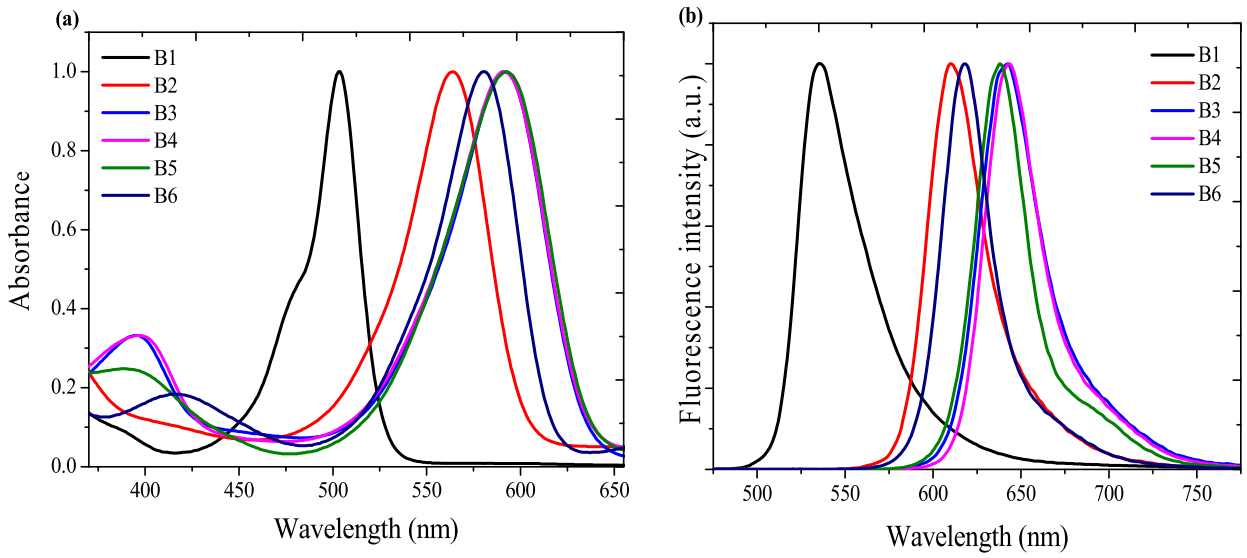

Fig. 2. Normalized **(a)** absorption and **(b)** fluorescence spectra of the dyes **B1**–**B6** in THF.

Table 2
Photophysical parameters of the BODIPYs in THF.

Compound	λ_{abs} (max/ nm)	λ_{ems} (max/ nm)	ε (M^{-1}. cm^{-1}) $\times 10^4$	FWHM (nm)	Stokes shifts $\Delta\nu_{ss}$ (nm)	[a]Φ_F
B1	504	536	1.47	30	32	0.236
B2	564	609	5.64	51	45	0.063
B3	592	642	5.93	60	50	0.066
B4	592	643	5.48	62	51	0.060
B5	594	640	5.94	62	46	0.117
B6	580	619	5.51	50	39	0.139

a: Fluorescein in ethanol ($\Phi_F = 0.79$) [33] was used as the fluorescence standard for the calculations of the fluorescence quantum yield and a correction was applied for the solvent refractive index (η) [THF: η = 1.4072, EtOH: 1.3614].

pronounced and narrow absorption band at 504 nm, corresponding to the S_0–S_1 (π -π*) transition, accompanied by a shoulder attributed to the 0−1 vibrational band of the same transition (Fig. 2-a). Additionally, absorption bands that are less intense and more broadened were observed below 400 nm, which correspond to transitions involving higher energy levels (S_0–S_2, etc.). The experimentally determined absorption maxima within the UV/vis spectra of the compounds range from 504 to 594 nm, contingent upon the presence of aromatic groups at the 1,3,5,7-positions of the BODIPY core. The presence of aromatic groups at the 1,3,5,7-positions is responsible for shifting the absorption bands by 60–90 nm towards the red region. The substitution of phenyl groups in place of hydrogen atoms resulted in a bathochromic shift of 60 nm, while the introduction of additional methoxy and naphthyl groups on the phenyl rings further augmented the bathochromic effect by approximately 30 nm. The observed red shift effect induced by the methoxyphenyl and naphthyl groups at the 1,7-positions manifests similarly within the absorption spectra. In the case of compounds **B5** and **B6**, the absence of phenyl groups at the *meso* (8) position of the core structure results in a bathochromic shift of approximately 90 nm and 76 nm, respectively. This shift is attributable to the reduction in steric hindrance observed in compounds **B5** and **B6**. In light of the molar absorption coefficients (ε), it can be inferred that the incorporation of aromatic phenyl/biphenyl groups results in a three to four-fold enhancement in absorptivity values compared to **B1** as reference, which correlates with the augmented conjugation values and an increase in the full width at half maximum (FWHM). Therefore, an increase in conjugation by aryl groups on the BODIPY core not only enhances the absorption intensities but also facilitates the effective absorption of wavelengths, particularly within the range of 450–650 nm, as a consequence of band broadening (FWHM).

Upon evaluation of the fluorescence spectra of the compounds, it was ascertained that the absorption and fluorescence bands exhibited mirror-image symmetry, indicative of the $S_1 \rightarrow S_0$ transition of the BODIPYs and the associated emission (Fig. 2-b). The emission of compound **B1** is detected at 536 nm, whereas the emissions of aryl-substituted derivatives range from 609 to 640 nm. The incorporation of electron-donating methoxy groups and aryl groups has been found to decrease the emission wavelength and the fluorescence quantum yields (Φ_F). The compounds exhibit fluorescence with quantum yields (Φ_F) ranging from 0.236 to 0.06, contingent upon the substitution of hydrogen, phenyl, methoxyphenyl, naphthyl or biphenyl groups. The observations can be attributed to the nonradiative energy dissipation occurring through rotation around C-phenyl bonds and the extension of π conjugation [29,30,32]. Furthermore, an increment ranging between 32 and 51 nm in the Stokes shifts ($\Delta\nu_{ss}$) of the compounds has been observed. This observation correlates with the increased conjugation, leading to π-π* and n-π* transitions, as a result of the augmented presence of aromatic groups conjugated to the BODIPY core within the planar BODIPY framework. It has been determined that enhancing the Stokes shifts, despite their drawbacks in BODIPYs due to factors such as peak interference, overlap/convolution, and self-quenching, may present benefits in photovoltaic applications. The incorporation of phenyl, biphenyl, and naphthyl substituents within the molecular structures examined in the study facilitates effective absorption within the visible spectrum, as evidenced by the absorption spectra. Moreover, the integration of aromatic moieties may diminish the reactivity of pyrrole rings or their susceptibility to nucleophilic/electrophilic attacks and photodegradation.

3.3. *Femtosecond transient absorption spectroscopy measurements*

In an attempt to find out the effect of the carboxy-biphenyl groups (compounds **B5** and **B6**) at the distal and proximal positions on the nonlinear absorption dynamics of the BODIPY core, femtosecond transient absorption spectroscopy measurements were carried out using an ultrafast pump-probe spectroscopy technique. The pump wavelength was chosen on the linear absorption spectra. In transient absorption spectra of compound **U1** in THF, there is a negative absorption signal at 685 nm corresponding to ground state bleaching (GSB). In addition, there are positive signals localized below 620 nm which can be ascribed to excited-state absorption (ESA) as shown in Fig. 3a.

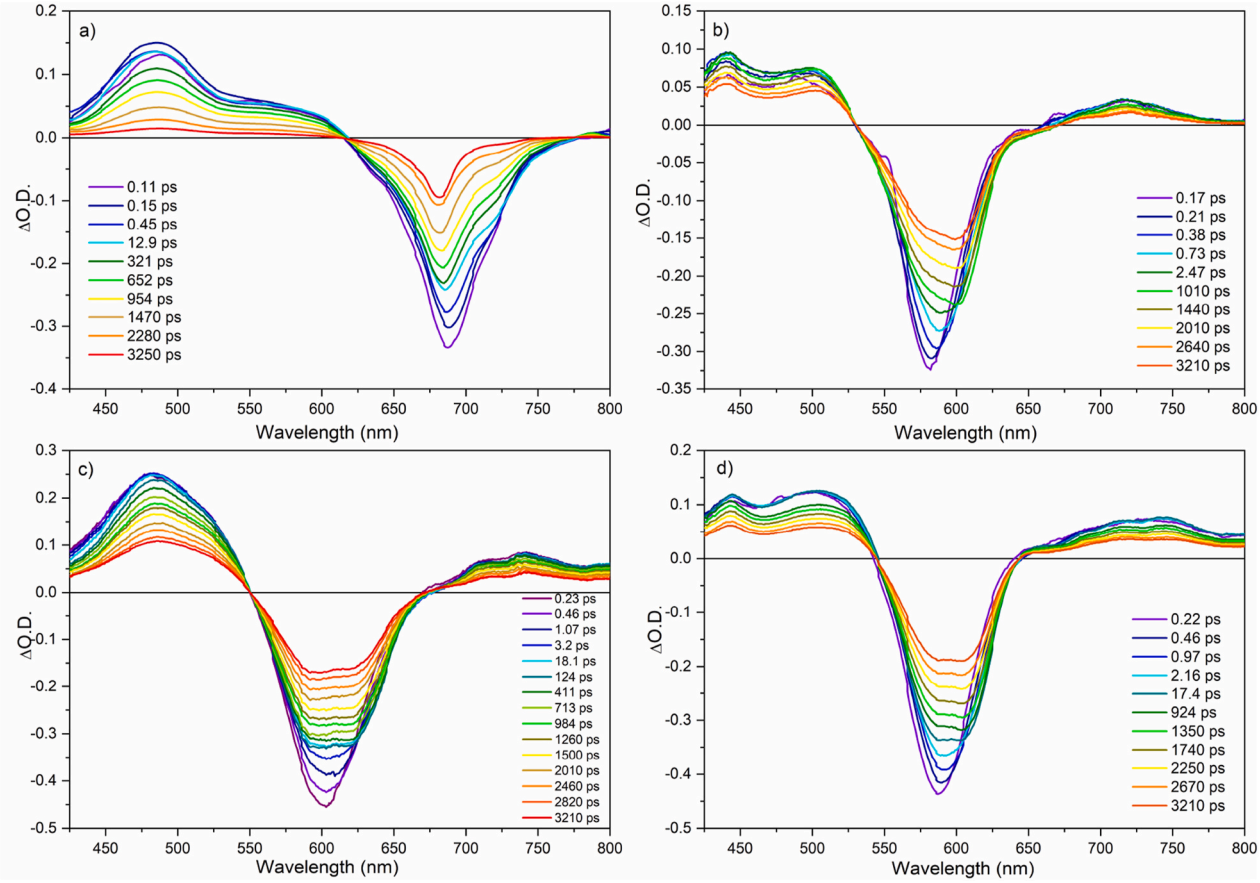

Fig. 3. Transient absorption spectra of a) **U1**, b) **U2**, c) **B5** and d) **B6** compounds in THF.

Upon photoexcitation at 575 nm, the GSB signal is localized around 580 nm, and the ESA signal was observed below 530 nm and above 660 nm for the **U2** compound. On the other hand, in the transient absorption spectra of the **B5** compound, the GSB signal appears around 600 nm, and ESA signals are seen below 550 nm and above 675 nm as indicated in Fig. 3c. Besides, the compound **B6** demonstrates similar transient absorption spectra upon photoexcitation at 580 nm wavelength.

To determine the excited state lifetime, the decay kinetics of the studied compound were fitted by using a multiexponential fitting function. The time evolution of the ground state bleaching signals for the studied compounds in THF solution is shown in Fig. 4.

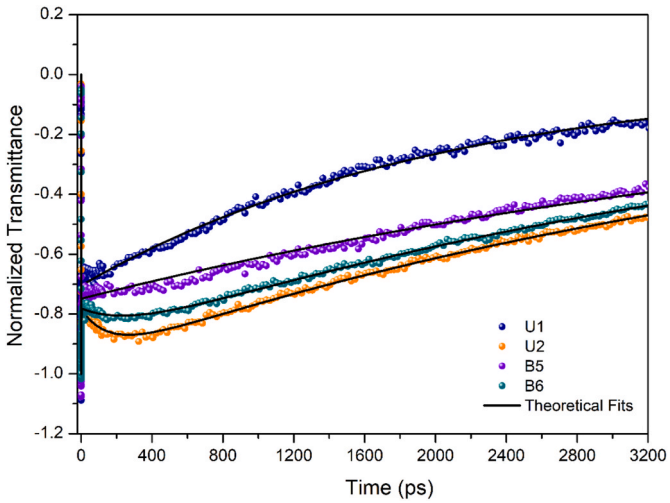

Fig. 4. Time evaluation spectra of the **U1**, **U2**, **B5** and **B6** compounds in THF.

According to the fitting results, the lifetime of the singlet excited state is shortened for the 3,5 (proximal) positions as compared to 1,7-(distal) positions. This shows the proximal positions (compound **B5**) are more efficient for the intramolecular charge transfer compared to the distal positions (compound **B6**) among the investigated compounds. Also, the dihedral angles between the BODIPY core and carboxybiphenyl groups for the distal positions are larger than those for the proximal positions by referring to the DFT calculation discussed in the previous section. Therefore, larger dihedral angles reduce orbital interferences, resulting in a hypsochromic shift in linear absorption (λ_{abs} max: 594 nm and 580 nm for compounds **B5** and **B6**, respectively). Thus, the charge transfer features resulting from the improved planarity of compound **B5** are enhanced upon photoexcitation compared to **B6**.

3.4. *Computational studies on photophysical properties of the compounds*

The computational calculations based on density functional theory (DFT) provide consistent results in elucidating the experimental photophysical characteristics of BODIPY compounds as documented in the literature [42–44]. This methodology was employed to determine the structure-absorption relationships of these compounds.

The theoretical data, including dipole moments (μ), electronic excitation energies (E_v), oscillator strengths (*f*), and main configurations, are summarized in Table 3, while the optimized structures, density of states (DOS) spectra, and natural transition orbitals (NTOs) of the BODIPYs are shown in Fig. 5. The optimization results indicated that in all compounds, the BODIPY core maintained a planar configuration while the complexes exhibited a pseudo-tetrahedral geometry.

Structurally, it was noted that the carboxyphenyl moieties at the *meso* (8) positions deviated from coplanarity with respect to the BODIPY

Table 3
Dipole moments (μ), electronic excitation energies (E_v), corresponding oscillator strengths (*f*), and the main configurations of the low-lying electronic excited states of the compounds.

Compound	Dipole moment μ/Debye	Electronic transition	Vertical excitation energy eV/nm	Oscillator Strength *f*	Major Contribution
B1	6.37	$S_0 \rightarrow S_1$	2.90/427	0.42	HOMO → LUMO (92 %)
		$S_0 \rightarrow S_2$	3.46/358	0.13	H−1 → LUMO (90 %)
		$S_0 \rightarrow S_3$	3.61/343	0.25	H−2 → LUMO (92 %)
B2	4.33	$S_0 \rightarrow S_1$	2.33/533	0.74	HOMO → LUMO (99 %)
		$S_0 \rightarrow S_2$	2.63/470	0.02	H−1 → LUMO (99 %)
		$S_0 \rightarrow S_3$	2.85/435	0.02	H−2 → LUMO (99 %)
B3	3.22	$S_0 \rightarrow S_1$	2.12/583	0.69	HOMO → LUMO (98 %)
		$S_0 \rightarrow S_2$	2.30/540	0.07	H−1 → LUMO (97 %)
		$S_0 \rightarrow S_3$	2.50/495	<0.01	H−2 → LUMO (98 %)
B4	4.95	$S_0 \rightarrow S_1$	2.10/590	0.62	HOMO → LUMO (95 %)
		$S_0 \rightarrow S_2$	2.27/546	0.04	H−1 → LUMO (98 %)
		$S_0 \rightarrow S_3$	2.39/518	0.07	H−2 → LUMO (96 %)
B5	11.40	$S_0 \rightarrow S_1$	2.15/577	0.96	HOMO → LUMO (99 %)
		$S_0 \rightarrow S_2$	2.78/446	0.01	H−2 → LUMO (96 %)
		$S_0 \rightarrow S_3$	2.89/429	0.79	H−1 → LUMO (76 %)
B6	3.73	$S_0 \rightarrow S_1$	2.21/562	0.91	HOMO → LUMO (98 %)
		$S_0 \rightarrow S_2$	2.67/465	<0.01	H−1 → LUMO (97 %)
		$S_0 \rightarrow S_3$	2.75/451	0.59	H−2 → LUMO (98 %)

core. The dihedral angles between the planar structure of the BODIPY core and the carboxyphenyl subunits at the *meso* (8) position were determined to be 49°, 63°, 65°, and 67° for the compounds **B1–B4**, respectively. The dihedral angles between the BODIPY core and the aryl groups at distal (1/7) positions are 50°, 56°, and 74° for the **B2–B4** compounds, respectively. In contrast, the corresponding angles for the **B5** and **B6** compounds are determined to be 36° and 41°, respectively. Consequently, one may discuss the steric influence of the aryl substituents positioned distally at the 1/7 positions of the core structure.

As expected, the steric effects imposed by the aromatic rings within compounds **B5** and **B6** are reduced owing to the lack of substituents at the *meso* (8) position. While the phenyl and methoxy phenyl groups exhibit a similar impact, the orientation becomes nearly perpendicular when naphthyl groups are present in compound **B4**. Upon considering the proximal positions (3,5), the dihedral angles for the compounds **B2–B6** were observed to be 37°, 34°, 36°, 35°, and 36°, respectively. It is noteworthy that compound **B1** was excluded from this analysis owing to the presence of a hydrogen atom. The dihedral angles demonstrated minimal variability in response to different substituents in proximal positions. This indicates that the groups in the proximal position (3,5) adopt a position slightly closer to the BODIPY plane than those in the distal (1,7) position. Therefore, the substituted groups in the proximal positions may be decisive on the conjugation.

Upon comparing the absorption wavelengths of compounds **B5** and **B6**, which are 594 nm and 580 nm respectively, the underlying cause of the observed spectral shift becomes apparent. Concerning the dipole moments of the molecules, which can be correlated with the polarities of the compounds, compound **B5** exhibits the highest polarity with a dipole moment of 11.40 Debye. This is attributed to the localization of all electronegative fluorine, nitrogen, and oxygen atoms within the proximal part of the molecule. In contrast, compound **B6**, wherein the carboxyphenyl groups occupy distal positions, has a dipole moment of 3.73 Debye.

The main (the lowest energy) singlet transitions of the compounds include HOMO-LUMO excitations, and for the upper energy levels, HOMO-1 and HOMO-2 type molecular orbitals also come into play. When the oscillator strengths (*f*) are considered, there is a notable agreement between the experimental and theoretical spectral patterns. A quantitative evaluation can be performed by computing the ratio of the experimental to theoretical absorption wavelengths ($\lambda_{exp}/\lambda_{cal}$). Consequently, the pertinent ratios for the compounds **B1–B6** are found to be 1.18, 1.06, 1.01, 1.00, 1.03, and 1.03, respectively. The energy band gaps ($\Delta E = |E_{HOMO} - E_{LUMO}|$) for the compounds reflected decreasing transition energies, which is in good agreement with the red-shifted absorption and emission wavelengths depending on the increased aromatic conjugation by substituted phenyl groups. The experimental spectra of the compounds dramatically reveal a striking 90 nm bathochromic shift between the maximum absorption peaks of **B1** and **B5**.

To visualize the main electronic transitions, natural transition orbitals (NTOs) were computed. These orbitals represent a combined depiction of excited electron-hole pairs derived from transition density matrices processed using TDDFT data. The main distribution regions of electrons and holes on the transition orbital isosurfaces were expressed in green and blue, respectively. The electrons for the main transition (S_0–S_1) states were exclusively localized on the BODIPY side. The singlet transitions are predominantly attributed to the phenyl and biphenyl rings located at the proximal (3,5) positions, particularly emphasizing the core structure of the molecules.

Due to electronic excitation, the charge density within the BODIPY core increased and even moved towards the *meso* (8) position in compound **B1**. The conjugation of this compound in the pyrrole rings is significant in terms of the absence of a restrictive group. However, it can be said that the charge density in the *meso* (8) position also increased in the **B2**–**B4** derivatives. In the **B5** and **B6** analogues, the electronegative carboxylic acid groups partially attract the charge density onto themselves.

As can be seen in the centroids of electrons and holes (C_{hole} & C_{ele}) in Table 4, the BODIPY core is affected to a large extent by the excitation. The presence of π-extended carboxyl subunits in the compounds increased the bathochromic effect and absorption bandwidths through conjugation.

In Table 4, the *t* index, a numerical value indicating the separation of the hole-electron couple, is positive when the hole/electron separation is clear. For the compounds **B1–B6**, the aforementioned values exhibit a systematic increase in the negative direction, specifically ranging from −0.489 to −2.155. This trend indicates a significant overlap between the holes and electron counterparts, and the S_0–S_1 transitions are

Compound	Total Energy (kcal/mol) x 10^3	Optimized structure	Density of states (DOS)
B1	691	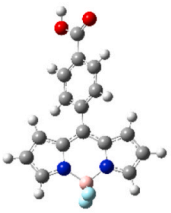	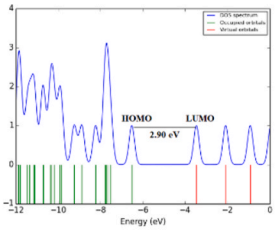
B2	1396	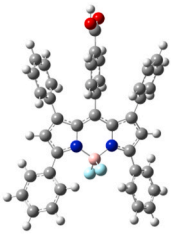	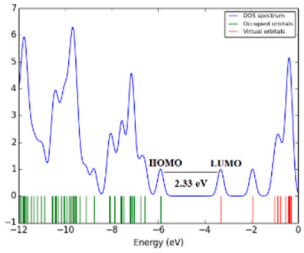
B3	1558	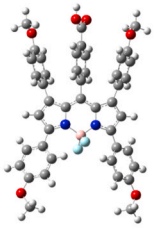	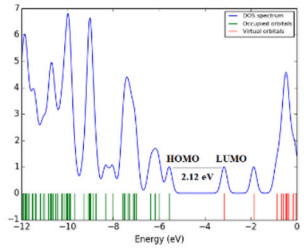
B4	1607	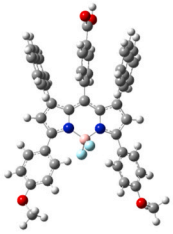	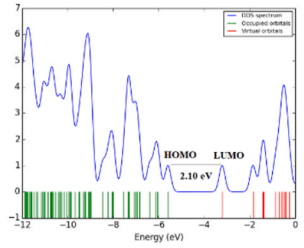
B5	1534	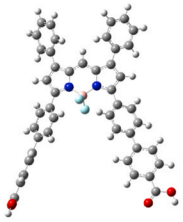	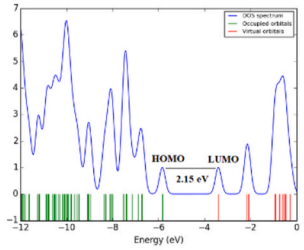
B6	1534	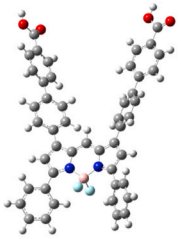	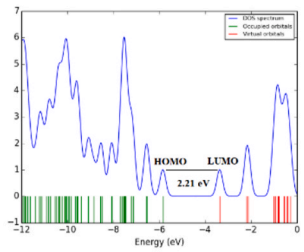

Fig. 5. Optimized structures and Density of states (DOS) spectra of the BODIPYs.

Table 4
Natural transition orbitals (NTOs) for the lowest-energy transitions of the BODIPYs (isosurface value = 0.02 au), centroids of hole and electron (C_{hole} & C_{ele}, isosurface value = 0.001 au).

Comp.	Transition	NTOs		C_{hole} & C_{ele}
		Electron	Hole	
B1	S_0–S_1 E_E: 2.90 eV *f*: 0.42 η: 1.52 eV χ: 4.98 eV ω: 8.16 eV *t* (Å): −0.489 E_C: 5.20 eV	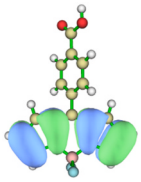	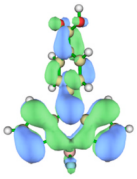	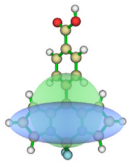
B2	S_0–S_1 E_E: 2.33 eV *f*: 0.74 η: 1.29 eV χ: 4.61 eV ω: 8.25 eV *t* (Å): −1.184 E_C: 4.13 eV	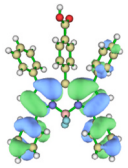	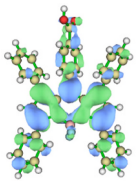	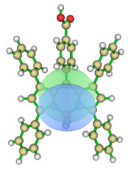
B3	S_0–S_1 E_E: 2.12 eV *f*: 0.69 η: 1.20 eV χ: 4.37 eV ω: 7.95 eV *t* (Å): −1.048 E_C: 3.61 eV	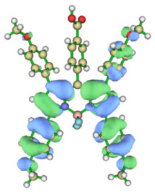	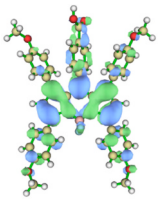	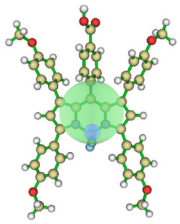
B4	S_0–S_1 E_E: 2.10 eV *f*: 0.62 η: 1.19 eV χ: 4.40 eV ω: 8.15 eV *t* (Å): −1.718 E_C: 3.56 eV	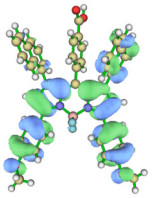	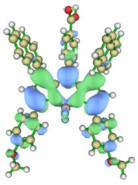	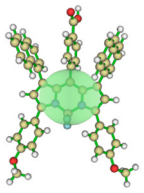
B5	S_0–S_1 E_E: 2.15 eV *f*: 0.96 η: 1.22 eV χ: 4.59 eV ω: 8.62 eV *t* (Å): −2.032 E_C: 3.56 eV	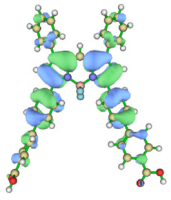	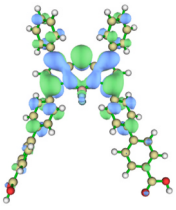	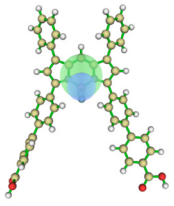
B6	S_0–S_1 E_E: 2.21 eV *f*: 0.91 η: 1.24 eV χ: 4.60 eV ω: 8.54 eV *t* (Å): −2.155 E_C: 3.71 eV	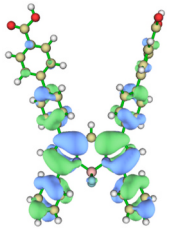	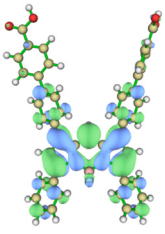	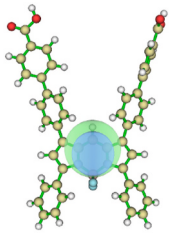

Blue and green isosurfaces represent C_{hole} and C_{ele} functions, respectively. *EE, f, and E_c represent the excitation energy, the oscillator strength, and the Coulomb attractive energy, respectively.* The t-index is a measure of the separation of the hole-electron in the charge transfer direction. η, χ and, ω represents the chemical hardness, electronegativity, and electrophilicity, respectively.

predominantly characterized by local excitations with n–π and π-π* features. This results in limited intramolecular charge transfer from the substituted groups to the BODIPY core.

Analogously, the Coulomb binding energies exceed the excitation energies required to facilitate the free movement of charges between electrons and holes. As a result, it was revealed that the main absorption bands of the BODIPYs were caused by intramolecular charge transfers. These charge transfers are not uniform throughout the molecule but occur with varying intensities depending on the substitution position of the carboxy-biphenyl groups on the on BODIPY core. The phenomenon of charge transfer is most pronounced at the proximal positions (3,5), diminishes at the *meso* (8) positions, and is least pronounced at the distal positions (1,7) of the BODIPY core.

3.5. Thermal properties

Thermogravimetry (TGA) is a technique wherein the mass of a sample is evaluated in relation to changes in temperature or time, through the application of a controlled temperature program [45,46]. Thermal resistance limits dye functionality, so we performed thermogravimetric analysis of compounds **B1–B6** to assess the efficiency of the BODIPYs in an inert N_2 atmosphere. The graphs depicting the time-dependent thermal degradation of the compounds are presented in Fig. 6, while the thermogram parameters are enumerated in Table 5. The thermal stability of the compounds is detailed through T_{max} (max decomposition speed temperature), decomposition rates at T_{max} (mass loss rate), percentage mass loss, T10 (10 % mass loss temperature), and C% (carbonization efficiency at 700 °C).

Based on the conducted measurements, the compounds demonstrate a 3 or 4-stage degradation profile within the temperature range of 200–1100 °C. Using compound **B1** as a point of reference, an elevation in the temperatures associated with maximum degradation (T_{max}) was generally noted in the other compounds.

Compound **B1**, lacking aromatic groups within its pyrrolic rings, commences degradation at approximately 284 °C, whereas the degradation temperatures for other compounds range between 212 and 345 °C. The most rapid mass loss among the compounds was observed at 212 °C for **B5**, whereas the corresponding thermal decomposition temperatures for compounds **B2**, **B3**, and **B4** were 345, 349, and 355 °C, respectively. At these temperatures, the compounds underwent decomposition at an approximate rate of 20 %.

The presence of aryl groups at pyrrolic sites enhanced the thermal stability of the compounds. Specifically, compound **B2** initiated degradation at 345 °C, with a decline in the rate of degradation from 3.79 (%/min) to 2.20 (%/min) in comparison to the reference. Such behavior was similarly observed in compounds **B3**, **B4**, and **B6**. Notably, compound **B5**, characterized by the incorporation of biphenyl-4-carboxylic acid at the 3,5 positions of the BODIPY core, exhibits the lowest thermal resistance within the series.

The T10 % values were utilized as the criterion for the comparative assessment of thermal stabilities, and the sequence was determined to be **B6** > **B2** > **B4** > **B3** > **B1** > **B5**. Despite the 3/5 positions on the BODIPY core being effective in terms of enhancing conjugation and consequently improving the photophysical properties of the molecule, the coupling reactions executed at these sites markedly diminished the thermal stability of the compounds. Conversely, the presence of these groups at the 1,7-positions contributed to an enhancement in thermal stability. Based on the carbonization efficiencies evaluated at 700 °C, it has been established that the phenyl groups directly bonded to the BODIPY core enhance thermal stability, whereas the phenyl groups located at the 3,5 positions notably diminish it. Furthermore, it is concluded that methoxy groups adversely affect thermal stability, particularly at lower T10 % decomposition temperatures (220–262 °C).

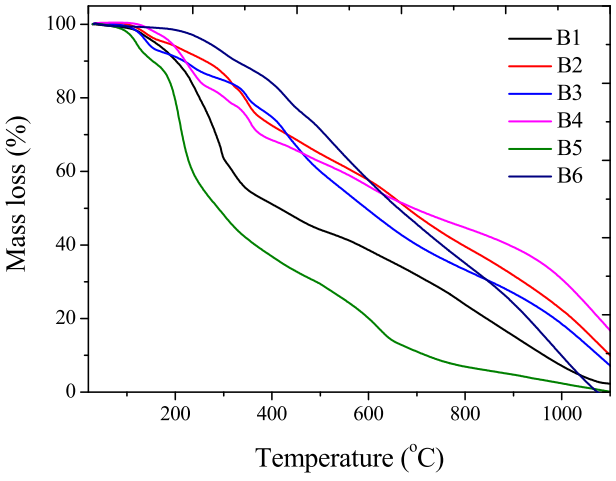

Fig. 6. Thermal decomposition of BODIPYs **B1**–**B6** at a temperature ramp of 10 °C/min under N_2.

Table 5
The decomposition temperatures and thermal stability of the compounds.

Compound	T_{max}(°C)[a]	Mass loss (%)	Decomposition rate (%/min)	[b]T10 % (°C)	[c]C %
B1	284	30	3.79	201	68
	454	53	0.77		
	598	61	0.65		
B2	345	20	2.20	262	52
	467	33	0.80		
	670	49	1.00		
B3	233	11	0.95	217	60
	349	20	2.00		
	423	28	1.84		
	601	51	1.00		
B4	227	11	2.08	220	50
	355	27	2.54		
	474	36	0.62		
	601	44	0.77		
B5	212	29	7.19	153	90
	305	53	1.71		
	620	83	1.33		
B6	302	8	1.02	326	54
	430	20	1.61		
	529	33	1.41		
	984	88	1.54		

[a] Maximum decomposition temperatures based on DTG plot.
[b] T10 % (temperature at which 10 % of initial mass is lost), etc.
[c] The carbonization efficiency (%) of the compounds at 700 °C.

4. Conclusions

In this study, we synthesized new symmetrical, conjugation-enhanced meso unsubstituted and aryl-substituted BODIPY dyes. The dyes incorporated aryl/carboxyl units at various positions within the core structure and were characterized utilizing spectroscopic techniques. The straightforward synthetic method potentially enables the conversion of active carboxyl termini into lipophilic ester or ether groups through further reactions. Alternatively, the formation of inorganic salts may be employed. These strategies could facilitate the improvement of water solubility and hold potential for utilization in cellular imaging and photodynamic therapy applications.

The electronic absorption and fluorescence properties of the compounds were systematically investigated using absorption and fluorescence spectroscopy techniques. The compounds exhibited primary absorption within the wavelengths of 504–594 nm and demonstrated fluorescence emissions ranging from 536 to 643 nm. These properties were contingent upon the enhanced conjugation through aryl subunits and the binding positions on the BODIPY core. The absorption bands were observed to have approximately doubled in width, spanning a range from 425 to 625 nm. The incorporation of substituted aryl groups at the 1,3,5,7-positions of the BODIPY core has been found to significantly enhance the photophysical properties, including the absorption and fluorescence wavelengths, molar absorptivity, and bandwidths, thereby facilitating panchromatic absorption. Conversely, the novel compounds exhibit moderate fluorescence quantum yields attributed to intramolecular charge transfers when contrasted with the methyl-substituted analogue. Notably, the increased Stokes shifts together with the pronounced bathochromic shifts observed in the main absorption and fluorescence bands of BODIPYs are considered advantageous as the red emitter for OLED, sensor and solar cell applications.

DFT calculations clarified spectral shifts in absorption and charge transfer, highlighting local excitations with n–π and π-π* transitions in BODIPY skeleton. Femtosecond transient absorption spectroscopy revealed that the singlet excited state lifetime is shorter for 3,5

(proximal) positions than 1,7- (distal) positions. Thus, proximal positions (compound **B5**) facilitate more efficient intramolecular charge transfer than distal positions (compound **B6**). Replacing hydrogen with phenyl groups at the 1,3,5,7-positions of the BODIPY skeleton significantly increased thermal stability (>150 °C). However, coupling reactions extending aryl groups at 3,5 positions decreased thermal stability. The enhanced thermal resistance of arylated carboxy-BODIPYs under comparatively "mild" conditions was considered to be of substantial importance for the fabrication of optical materials through physical methods necessitating thermal processing. It has been demonstrated that the π-extended carboxyl frameworks afford partial conjugation with the BODIPY chromophores, thereby significantly enhancing the characteristics of the practically significant spectral properties of these dyes. While the current investigation yielded symmetric BODIPYs, asymmetric compounds can also be synthesized utilizing pyrroles with varied substituents in the synthesizing of **U1** and **U2**, as the employed method permits such modifications. Our results may contribute to the design of novel BODIPY dyes with broad absorption and emission intervals with higher thermal and photostability which can be used as light-harvesting systems in nonlinear optical systems.

CRediT authorship contribution statement

Gökhan Sevinç: Writing – review & editing, Supervision, Software, Methodology, Investigation, Conceptualization. **Elif Akhüseyin Yıldız:** Writing – original draft, Methodology, Investigation, Formal analysis, Data curation. **Zeliha Pınar Taşkıran:** Investigation. **Ahmet Karatay:** Writing – original draft, Supervision, Investigation.

Declaration of competing interest

The authors declare that they have no known competing financial interests or personal relationships that could have appeared to influence the work reported in this paper.

Acknowledgments

This research has been funded by the Research Fund of Bilecik Seyh Edebali University (Project Number: 2022-02.BŞEÜ.35-02).

Appendix A. Supplementary data

Supplementary data to this article can be found online at https://doi.org/10.1016/j.dyepig.2025.112776.

Data availability

No data was used for the research described in the article.

References

[1] Ozcan E, Kazan HH, Çoşut B. Recent chemo-/biosensor and bioimaging studies based on indole-decorated BODIPYs. Luminescence 2020;35:168–77. https://doi.org/10.1002/bio.3719.
[2] Donnelly JL, Offenbartl-Stiegert D, Marín-Beloqui JM, Rizzello L, Battaglia G, Clarke TM, et al. Exploring the relationship between BODIPY structure and spectroscopic properties to design fluorophores for bioimaging. Chem Eur J 2020;26:863–72. https://doi.org/10.1002/chem.201904164.
[3] Kaur P, Singh K. Recent advances in the application of BODIPY in bioimaging and chemosensing. J Mater Chem C Mater 2019;7:11361–405.
[4] Malacarne MC, Gariboldi MB, Caruso E. BODIPYs in PDT: a journey through the most interesting molecules produced in the last 10 years. Int J Mol Sci 2022;23. https://doi.org/10.3390/ijms231710198.
[5] Prieto-Montero R, Prieto-Castañeda A, Sola-Llano R, Agarrabeitia AR, García-Fresnadillo D, López-Arbeloa I, et al. Exploring BODIPY derivatives as singlet oxygen photosensitizers for PDT. Photochem Photobiol 2020;96:458–77. https://doi.org/10.1111/php.13232.
[6] Awuah SG, You Y. Boron dipyrromethene (BODIPY)-based photosensitizers for photodynamic therapy. RSC Adv 2012;2:11169–83. https://doi.org/10.1039/C2RA21404K.
[7] Kamkaew A, Lim SH, Lee HB, Kiew LV, Chung LY, Burgess K. BODIPY dyes in photodynamic therapy. Chem Soc Rev 2013;42:77–88. https://doi.org/10.1039/C2CS35216H.
[8] Wang L, Ding H, Ran X, Tang H, Cao D. Recent progress on reaction-based BODIPY probes for anion detection. Dyes Pigments 2020;172:107857. https://doi.org/10.1016/j.dyepig.2019.107857.
[9] Bumagina NA, Antina EV. Review of advances in development of fluorescent BODIPY probes (chemosensors and chemodosimeters) for cation recognition. Coord Chem Rev 2024;505:215688. https://doi.org/10.1016/j.ccr.2024.215688.
[10] Xia H-C, Xu X-H, Song Q-H. BODIPY-based fluorescent sensor for the recognization of phosgene in solutions and in gas phase. Anal Chem 2017;89:4192–7.
[11] Boens N, Leen V, Dehaen W. Fluorescent indicators based on BODIPY. Chem Soc Rev 2012;41:1130–72.
[12] Yadav IS, Misra R. Design, synthesis and functionalization of BODIPY dyes: applications in dye-sensitized solar cells (DSSCs) and photodynamic therapy (PDT). J Mater Chem C Mater 2023;11:8688–723. https://doi.org/10.1039/D3TC00171G.
[13] Klfout H, Stewart A, Elkhalifa M, He H. BODIPYs for dye-sensitized solar cells. ACS Appl Mater Interfaces 2017;9:39873–89. https://doi.org/10.1021/acsami.7b07688.
[14] Yildiz EA, Sevinc G, Yaglioglu HG, Hayvali M. The effect of molecular structure and ultrafast electron injection dynamics on the efficiency of BODIPY sensitized solar cells. Opt Mater 2019;91:50–7. https://doi.org/10.1016/J.OPTMAT.2019.02.025.
[15] Squeo BM, Pasini M. BODIPY platform: a tunable tool for green to NIR OLEDs. Supramol Chem 2020;32:56–70. https://doi.org/10.1080/10610278.2019.1691727.
[16] Poddar M, Misra R. Recent advances of BODIPY based derivatives for optoelectronic applications. Coord Chem Rev 2020;421:213462. https://doi.org/10.1016/j.ccr.2020.213462.
[17] Squeo BM, Pasini M. BODIPY platform: a tunable tool for green to NIR OLEDs. Supramol Chem 2020;32:56–70. https://doi.org/10.1080/10610278.2019.1691727.
[18] Banfi S, Nasini G, Zaza S, Caruso E. Synthesis and photo-physical properties of a series of BODIPY dyes. Tetrahedron 2013;69:4845–56.
[19] Clarke RG, Hall MJ. Recent developments in the synthesis of the BODIPY dyes. Adv Heterocycl Chem 2019;128:181–261. https://doi.org/10.1016/BS.AIHCH.2018.12.001.
[20] Lakshmi V, Sharma R, Ravikanth M. Functionalized boron-dipyrromethenes and their applications. Rep Org Chem 2016;6:1–24. https://doi.org/10.2147/ROC.S60504.
[21] Lu H, Shen Z. BODIPYs and their derivatives: the past, present and future. Front Chem 2020;8:290.
[22] Loudet A, Burgess K. BODIPY dyes and their derivatives: syntheses and spectroscopic properties. Chem Rev 2007;107:4891–932. https://doi.org/10.1021/cr078381n.
[23] Ooyama Y, Harima Y. Photophysical and electrochemical properties, and molecular structures of organic dyes for dye-sensitized solar cells. ChemPhysChem 2012;13:4032–80. https://doi.org/10.1002/cphc.201200218.
[24] Mao M, Song Q. The structure-property relationships of D-π-A BODIPY dyes for dye-sensitized solar cells. Chem Rec 2016;16:719–33.
[25] Singh SP, Gayathri T. Evolution of BODIPY dyes as potential sensitizers for dye-sensitized solar cells. Eur J Org Chem 2014;2014:4689–707.
[26] Yildiz EA, Ünlü BA, Karatay A, Bozkurt Y, Özler ME, Sözmen F, et al. Two-Photon absorption response of functionalized BODIPY dyes in near-IR region by tuning conjugation length and meso-substituents. ACS Omega 2023;8:30939–48. https://doi.org/10.1021/acsomega.3c02314.
[27] Akhuseyin Yildiz E, Yabaş E, Sözmen F, Bozkurt Y, Karatay A, Boyacioglu B, et al. Effects of heavy iodine atoms and π-expanded conjugation on charge transfer dynamics in carboxylic acid BODIPY derivatives as triplet photosensitizers. ChemPhysChem 2023;24:e202200735. https://doi.org/10.1002/cphc.202200735.
[28] Gräf K, Körzdörfer T, Kümmel S, Thelakkat M. Synthesis of donor-substituted meso-phenyl and meso-ethynylphenyl BODIPYs with broad absorption. New J Chem 2013;37:1417–26. https://doi.org/10.1039/C3NJ00157A.
[29] Yildiz EA, Sevinç G, Tekin S, Karatay A, Hayvalı M, Elmali A. Great enhancement of two photon absorption cross section value by intramolecular charge transfer in newly synthesized triphenylamine-BODIPY derivative. Dyes Pigments 2021;193:109522. https://doi.org/10.1016/j.dyepig.2021.109522.
[30] Sevinç G, Küçüköz B, Elmalı A, Hayvalı M. The synthesis of −1, −3, −5, −7, −8 aryl substituted boron-dipyrromethene chromophores: nonlinear optical and photophysical characterization. J Mol Struct 2020;1206:127691. https://doi.org/10.1016/j.molstruc.2020.127691.
[31] Gawley RE, Mao H, Haque MM, Thorne JB, Pharr JS. Visible fluorescence chemosensor for saxitoxin. J Org Chem 2007;72:2187–91. https://doi.org/10.1021/jo062506r.
[32] Küçüköz B, Sevinç G, Yildiz E, Karatay A, Zhong F, Yılmaz H, et al. Enhancement of two photon absorption properties and intersystem crossing by charge transfer in pentaaryl boron-dipyrromethene (BODIPY) derivatives. Phys Chem Chem Phys 2016;18:13546–53.
[33] Kellogg RE, Bennett RG. Radiationless intermolecular energy transfer. III. Determination of phosphorescence efficiencies. J Chem Phys 1964;41:3042–5. https://doi.org/10.1063/1.1725672.
[34] Frisch R, Trucks GW, Schlegel HB, Scuseria GE, Robb MA, Cheeseman JR, et al. Gaussian09, 1 121, Gaussian. Wallingford CT: Inc; 2009. p. 150e166.
[35] Martin RL. Natural transition orbitals. J Chem Phys 2003;118:4775–7. https://doi.org/10.1063/1.1558471.
[36] Lu T, Chen F. Multiwfn: a multifunctional wavefunction analyzer. J Comput Chem 2012;33:580–92. https://doi.org/10.1002/jcc.22885.

[37] O'boyle NM, Tenderholt AL, Langner KM. cclib: a library for package-independent computational chemistry algorithms. J Comput Chem 2008;29:839–45. https://doi.org/10.1002/jcc.20823.
[38] Duan X, Li P, Li P, Xie T, Yu F, Tang B. The synthesis of polarity-sensitive fluorescent dyes based on the BODIPY chromophore. Dyes Pigments 2011;89:217–22. https://doi.org/10.1016/j.dyepig.2010.03.007.
[39] Wu L, Burgess K. A new synthesis of symmetric boraindacene (BODIPY) dyes. Chem Commun 2008:4933–5. https://doi.org/10.1039/B810503K.
[40] Li Z, Chen Y, Lv X, Fu W-F. A tetraphenylethene-decorated BODIPY monomer/dimer with intense fluorescence in various matrices. New J Chem 2013;37:3755–61. https://doi.org/10.1039/C3NJ00703K.
[41] Sevinç G, Küçüköz B, Yılmaz H, Şirikçi G, Yaglioglu HG, Hayvalı M, et al. Explanation of pH probe mechanism in borondipyrromethene-benzimidazole compound using ultrafast spectroscopy technique. Sensor Actuator B Chem 2014;193:737–44. https://doi.org/10.1016/j.snb.2013.12.043.
[42] Laine M, Barbosa NA, Wieczorek R, Melnikov MYa, Filarowski A. Calculations of BODIPY dyes in the ground and excited states using the M06-2X and PBE0 functionals. J Mol Model 2016;22:260. https://doi.org/10.1007/s00894-016-3108-8.
[43] Yildiz EA, Ünlü BA, Karatay A, Bozkurt Y, Özler ME, Sözmen F, et al. Two-Photon absorption response of functionalized BODIPY dyes in near-IR region by tuning conjugation length and meso-substituents. ACS Omega 2023;8:30939–48. https://doi.org/10.1021/acsomega.3c02314.
[44] Helal W, Marashdeh A, Alkhatib Q, Qashmar H, Gharaibeh M, Afaneh AT. Tuning the photophysical properties of BODIPY dyes used in DSSCs as predicted by double-hybrid TD-DFT: the role of the methyl substituents. Int J Quant Chem 2022;122:e27000. https://doi.org/10.1002/qua.27000.
[45] Bumagina NA, Ayu Kritskaya, Antina EV, Berezin MB, V'yugin AI. Effect of alkyl, aryl, and meso-aza substitution on the thermal stability of BODIPY. Russ J Inorg Chem 2018;63:1326–32. https://doi.org/10.1134/S0036023618100030.
[46] Coats AW, Redfern JP. Thermogravimetric analysis. A review. Analyst 1963;88:906–24. https://doi.org/10.1039/AN9638800906.